CONF-900617--15

Study of the Influence of Imperfections on the Dynamic Stability of Tanks*

by

Rasim Aziz Uras
Reactor Safety and Analysis Division
Argonne National Laboratory
Argonne, Illinois 60439

CONF-900617--15

DE90 011094

and

Wing Kam Liu and Yi-Jung Chen
Department of Mechanical Engineering
Northwestern University
Evanston, IL 60208

ASME Pressure Vessels and Piping Conference,
Nashville, TN, June 17-21, 1990

*Work supported by the U.S. Department of Energy, Office of Technology Support Programs under Contract W-31-109-Eng-38.

Center across both columns on page 1: Title, Authors, Affiliations

Study of the Influence of Imperfections on the Dynamic Stability of Tanks

by

Rasim Aziz URAS
Reactor Safety and Analysis Division
Argonne National Laboratory
Argonne, IL 60439

and

Wing Kam LIU and Yi-Jung CHEN
Department of Mechanical Engineering
Northwestern University
Evanston, IL 60208

Page 1: Title, Authors, Affiliations

Start page 1, beginning with abstract

Abstract

The influence of geometrical imperfections on the dynamic stability of liquid-filled shells under horizontal ground excitation is studied. Some basic concepts in the large deformation and large deformation thin shell theory are recalled. The work done by inertial and internal forces are given in the Gaussian surface coordinate system. A general imperfection pattern in the circumferential direction is introduced. The emphasis is particularly dedicated to the analysis of the geometrical stiffness term. Different patterns are studied to explain the occurrence of additional instability regions.

1.Introduction

A method of analysis for the dynamic stability of liquid-filled shells under earthquake excitation has been introduced by Liu and Uras (1989a). They have derived the discrete fluid-structure interaction equations through the use of a Galerkin/Finite element procedure. Applications of this analysis for various loading cases, including horizontal ground motion have been studied in Liu and Uras (1989b).

A comparison of experimental findings by Chiba et al. (1986) with the theoretical analysis by Liu and Uras (1989a) has been discussed in Uras and Liu (1990). The analysis by Liu and Uras (1989a) yields the same buckling frequencies due to the (n)th and (n+1)th circumferential modal coupling as the experiments. It is also found that each of the experimental instability regions consists of many regions due to various axial and circumferential modal coupling. The reasons for the occurrence of instability regions other than the circumferential modal coupling are stated. However, the theory presented Liu and Uras (1989a) is not able to explain the instability regions of higher order circumferential coupling, i.e. between (n)th and (n+k)th where k is an integer. It is believed that these regions originated from the geometrical imperfections in the shell. The present work intends to shed some light into the influence of various imperfection patterns on the dynamic stability.

Preliminaries on the large deformation and large rotation theory of thin shells, and stress and strain measures are given in Section 2. In Section 3, the linearization of the virtual work principle for inertial and internal forces is briefly mentioned. The geometrical stiffness term is handled in some detail since this term plays an important role in the stability analysis. In Section 4, comparison of results between the analyses of Liu and Uras (1989a), Uras and Liu (1990) and the experimets of Chiba et al. (1986) are presented. In Section 5, an imperfection pattern in the circumferential direction is considered, and an asymptotic expansion for the geometrical stiffness term in terms of the imperfection amplitude is given. The influence of the sinuzoidal patterns on the stability are analyzed in Section 6.

2.Preliminaries

The middle-surface of a thin shell is described by the Gaussian coordinates, ξ^1 and ξ^2 (Sanders (1963), Koiter (1966)) where they can be chosen to be the axial and circumferential directions in a cylindrical coordinate system, i.e.

$$\xi^1 = z \qquad \xi^2 = \theta \tag{2.1}$$

The position vector, $\mathbf{r}$, from the origin of a fixed cylindrical coordinate system to a generic point on the middle-surface of the undeformed shell can be given as

$$\mathbf{r} = R(z,\theta)\,\mathbf{e}_r + z\,\mathbf{e}_z \tag{2.2}$$

where $\mathbf{e}_r$, $\mathbf{e}_\theta$ and $\mathbf{e}_z$ are the unit vectors in the radial, circumferential and axial directions, respectively.
The covariant surface base vectors are defined by

$$\mathbf{r}_{,\alpha} = \frac{\partial \mathbf{r}}{\partial \xi^\alpha} \qquad \alpha = 1,2 \tag{2.3}$$

Hence, the unit normal to the surface is obtained from the cross-product of the base vectors:

$$\mathbf{n} = \frac{\mathbf{r}_{,1} \times \mathbf{r}_{,2}}{|\mathbf{r}_{,1} \times \mathbf{r}_{,2}|} \tag{2.4}$$

The first and second fundamental tensors of the undeformed middle surface can be given as

$$g_{\alpha\beta} = \mathbf{r}_{,\alpha} \cdot \mathbf{r}_{,\beta} \tag{2.5}$$

and

$$b_{\alpha\beta} = \mathbf{n}_{,\alpha} \cdot \mathbf{r}_{,\beta} \tag{2.6}$$

respectively; the respective determinants will be denoted by g and b. A differential surface element is described by

$$d\Gamma = \sqrt{g}\; d\xi^1 d\xi^2 \tag{2.7}$$

Since the surface base vectors generally do not constitute an orthogonal set, the changes in tensorial quantities are described by covariant derivatives

$$v^{\alpha}{}_{|\beta} = v^{\alpha}{}_{,\beta} + \Gamma^{\alpha}_{\lambda\beta}\, v^{\lambda} \tag{2.8}$$

and

$$T^{\alpha\beta}{}_{|\mu} = T^{\alpha\beta}{}_{,\mu} + \Gamma^{\alpha}_{\lambda\mu}\, T^{\lambda\beta} + \Gamma^{\beta}_{\lambda\mu}\, T^{\alpha\lambda} \tag{2.9}$$

where v and T denote first and second order tensors, respectively, and a repeated subscript-superscript implies summation. $\Gamma^{\alpha}_{\lambda\mu}$ designates the Christoffel symbols of the second kind:

$$\Gamma^{\alpha}_{\lambda\mu} = g^{\xi\lambda}\,\Gamma_{\lambda\alpha\beta} \quad ; \quad \Gamma_{\lambda\alpha\beta} = \frac{1}{2}\left(g_{\lambda\alpha,\beta} + g_{\lambda\beta,\alpha} - g_{\alpha\beta,\lambda}\right) \tag{2.10}$$

After the shell undergoes a deformation, the new position vector, $\tilde{\mathbf{r}}$, to the deformed middle surface is given by

$$\tilde{\mathbf{r}} = \mathbf{r} + \mathbf{u} \tag{2.11}$$

where the displacement vector, **u**, is defined through its components along the directions of the base vectors and unit normal vector, and are denoted by u^{α} and w, respectively:

$$\mathbf{u} = u^{\alpha}\,\mathbf{r}_{,\alpha} + w\,\mathbf{n} \tag{2.12}$$

The strain tensor is defined through the metric tensors $\tilde{g}_{\alpha\beta}$ and $g_{\alpha\beta}$ of the deformed and undeformed middle surfaces, respectively

$$E_{\alpha\beta} = \frac{1}{2}\left(\tilde{g}_{\alpha\beta} - g_{\alpha\beta}\right) \tag{2.13}$$

The stress tensor can be related to the strain tensor through the use of the elasticity tensor $C^{\alpha\beta\gamma\lambda}$

$$S^{\alpha\beta} = C^{\alpha\beta\gamma\lambda}\, E_{\gamma\lambda} \tag{2.14}$$

The curvature tensor is defined through the metric tensors $\tilde{b}_{\alpha\beta}$ and $b_{\alpha\beta}$ of the deformed and undeformed middle surfaces, respectively

$$K_{\alpha\beta} = \frac{1}{2}\left(\tilde{b}_{\alpha\beta} - b_{\alpha\beta}\right) \tag{2.15}$$

The moment tensor can be related to the curvature tensor through the use of the elasticity tensor $C^{\alpha\beta\gamma\lambda}$

$$M^{\alpha\beta} = C^{\alpha\beta\gamma\lambda}\, K_{\gamma\lambda} \tag{2.16}$$

3.Linearization of virtual work term

The virtual work done by the inertial forces consists of two parts representing the shell inertial effects and the fluid added inertia, I_i^{ad}

$$\delta\Pi^{I} = \int_{\Gamma} \left[\, h\rho\, \delta u_i\; \ddot{u}_i + \delta u_i\; I_i^{ad} \,\right] d\Gamma \qquad i=1,3 \tag{3.1}$$

where a superposed dot denotes the temporal derivative

The virtual work done by a thin shell undergoing a small strain, large deformation and large rotations can be expressed as

$$\delta\Pi = \int_{\Gamma} \left[\, h\, \delta E_{\alpha\beta}\, S^{\alpha\beta} + \frac{h^3}{12}\, \delta K_{\alpha\beta}\, M^{\alpha\beta} \,\right] d\Gamma \qquad \alpha,\beta = 1,2 \tag{3.2}$$

where h is the shell thickness.

The contibution of the material effects to the work done by internal forces yields the material stiffness term

$$\delta\Pi^{D} = \int_{\Gamma} \left[\, h\, \delta E_{\alpha\beta}\, L[S^{\alpha\beta}] + \frac{h^3}{12}\, \delta K_{\alpha\beta}\, L[M^{\alpha\beta}] \,\right] d\Gamma \qquad \alpha,\beta = 1,2 \tag{3.3}$$

where L[.] is the linearization operator.

The effect of the initial stresses and moments is represented by the geometrical stiffness term. The identification of modal coupling, and its influence on determining the buckling criteria are possible through studying the geometrical stiffness matrix (Liu and Uras (1989a)). Thus, the treatment of this stiffness term will be given in more detail:

$$\delta\Pi^{G} = \int_{\Gamma} \left[\, h\, L[\delta E_{\alpha\beta}]\, S^{\alpha\beta} + \frac{h^3}{12}\, L[\delta K_{\alpha\beta}]\, M^{\alpha\beta} \,\right] d\Gamma \tag{3.4}$$

where $S^{\alpha\beta}$ and $M^{\alpha\beta}$ are interpreted as the initial stress and the initial moment tensors, respectively. The initial moment term is eliminated due to its negligible contribution to the overall stability response.

The linearized strain tensor can be expressed in terms of the displacement vector

$$L[\delta E_{\alpha\beta}] = \delta u_{,\alpha} \cdot \Delta u_{,\beta} \tag{3.5}$$

The displacement components can be discretized using their respective mode shapes

$$u^1(z,\theta,t) = \sum_{i=1}^{I} \sum_{n=0}^{N} u_{in}(t)\; U_i(z)\; \bar{U}_n(\theta) \tag{3.6a}$$

$$u^2(z,\theta,t) = \sum_{i=1}^{I} \sum_{n=0}^{N} v_{in}(t)\; V_i(z)\; \bar{V}_n(\theta) \tag{3.6b}$$

$$w(z,\theta,t) = \sum_{i=1}^{I} \sum_{n=0}^{N} w_{in}(t)\; W_i(z)\; \bar{W}_n(\theta) \tag{3.6c}$$

where ξ^{α} are replaced by z and θ. Following similar guidelines presented in Liu and Uras (1989a), the geometrical stiffness matrix is obtained

$$K^{G}_{ijnm} = \int_0^L h\,(B_{zi})^T \left[\int_0^{2\pi} (B_{n\theta})^T\, S\, (B_{m\theta})\, \sqrt{g}\; d\theta \right] (B_{zj})\; dz \tag{3.7}$$

where the matrices are tabulated in Table 3.1. For a geometrically perfect shell Eqn. (3.7) reduces to its counterpart given in Liu and Uras (1989a).

4.Comparison of Results and Stability Charts

The results for a 75% full tall shell obtained from the analysis of Liu and Uras (1989b) and Uras and Liu (1990) are compared to

those of the experimental study by Chiba et al. (1986). Stability chart (a) is established by applying the constant maximum membrane stress criterion presented in Liu and Uras (1989b). Stability chart (b) represents the results obtained through the new method proposed in Uras and Liu (1990) which is based on evaluating the membrane forces through the use of horizontal ground acceleration. The experimental results by Chiba et al. (1986) are duplicated in the stability chart (c). In order to obtain all relevant buckling frequencies, a small amount of damping ($\zeta_{min} = 0.1\%$) is used in the present analysis.

Experimental and theoretical values of the first cosθ-mode are 110 Hz. and 115 Hz., respectively. Major buckling modes around this mode are identified as cos9θ and cos10θ. The comparison of results by Liu and Uras (1989b), the present analysis and Chiba et al. (1986) experiments are depicted in Figures 4.1a, 4.1b, and 4.1c, respectively. The instability regions within the frequency scattering in the vicinity of the first cosθ-mode are summarized as follows:

Within a ±10% margin of the (1,1) cosθ-mode frequency, i.e. ω_{11}=115 Hz., the shell will buckle with $\varepsilon_{cr} \le 0.4$ at the following mode shapes and frequencies (see Figures 4.1a and 4.1b, and Table 4.1a, the numbers are highlighted by bold italics):

a) axial mode (1,1) and circumferential mode coupling (2,3) and at frequencies (67 and 43 Hz.);
b) axial mode (1,2) and circumferential mode coupling (6,7) and at frequencies (31 and 81 Hz.);
c) axial mode (1,2) and circumferential mode coupling (5,6) and at frequencies (28 and 87 Hz.);
d) axial mode (1,1) and circumferential mode coupling (9,10) and at frequencies (53 and 63 Hz.);
e) axial mode (1,2) and circumferential mode coupling (7,8) and at frequencies (37 and 83 Hz.);
f) axial mode (2,1) and circumferential mode coupling (6,7) and at frequencies (87 and 37 Hz.);

As can be seen from Figures 4.1, the above six buckling mode shapes (as indicated by the first thick curve in Figures 4.1a and 4.1b) obtained from Uras and Liu (1990) agree with the region obtained by Chiba et al. as shown in Figure 4.1c. From their experiment, they can identify only the axial mode (1,1) and the circumferential mode (9,10). Therefore, the buckling modes cannot be precisely determined from their shaking table experiments.

The locations of the instability regions representing the axial mode (1,1) and the (n)th and (n+1)th circumferential modal coupling obtained through the present analysis and from Chiba et al. (1986) are tabulated in Table 4.1b. The difference in predicting the buckling frequencies is within 1.8 % of those by Chiba et al. (1986). It should be noted that only six buckling frequencies are available for comparison (see Figures 4.1).

5.Influence of imperfection on the dynamic stability

For a geometrically perfect shell the base vectors and the unit normal of the middle surface coincide with the cylindrical coordinate directions. However, the addition of an imperfection necessitates the use of the large deformation theory, briefly outlined in the preliminaries section.

In this study, an imperfection pattern only in the circumferential direction will be considered:

$$R = \bar{R}\,[1 + \mu\, f(\theta)\,] \tag{5.1}$$

where $\bar{R}$ is the average radius, μ is the normalized imperfection amplitude, and f represents the spatial imperfection pattern.

Some of the terms in Eqn. (3.7) can be expanded in μ

$$B_{n\theta} = B^0_{n\theta} + \mu\, B^1_{n\theta} + \mu^2\, B^2_{n\theta} + O(\mu^3) \tag{5.2}$$

$$S = S_0 + \mu\, S_1 + \mu^2\, S_2 + O(\mu^3) \tag{5.3}$$

where the matrices are tabulated in Table 5.1. After substituting Eqns. (5.2) and (5.3) into Eqn. (3.7), a second-order expansion for the geometrical stiffness matrix is obtained

$$K^G = K^G_0 + \mu\, K^G_1 + \mu^2\, K^G_2 + O(\mu^3) \tag{5.4}$$

where

$$K^G_0 = \int_0^L h\,(B_{zi})^T \left[\int_0^{2\pi} (B^0_{n\theta})^T\, S_0\, (B^0_{m\theta})\, d\theta \right] (B_{zj})\, dz \tag{5.5}$$

$$K^G_1 = \int_0^L h\,(B_{zi})^T \left[\int_0^{2\pi} (B^0_{n\theta})^T\, S_0\, (B^1_{m\theta}) + (B^1_{n\theta})^T\, S_0\, (B^0_{m\theta}) + (B^0_{n\theta})^T\, S_1\, (B^0_{m\theta})\, d\theta \right] (B_{zj})\, dz \tag{5.6}$$

$$K^G_2 = \int_0^L h\,(B_{zi})^T \left[\int_0^{2\pi} (B^0_{n\theta})^T\, S_2\, (B^0_{m\theta}) + (B^0_{n\theta})^T\, S_1\, (B^1_{m\theta}) + (B^0_{n\theta})^T\, S_0\, (B^2_{m\theta}) + (B^1_{n\theta})^T\, S_1\, (B^0_{m\theta}) + (B^1_{n\theta})^T\, S_0\, (B^1_{m\theta}) + (B^2_{n\theta})^T\, S_0\, (B^0_{m\theta})\, d\theta \right] (B_{zj})\, dz \tag{5.7}$$

6. A special case

Assume that the imperfection can be characterized by one sinuzoidal function

$$f(\theta) = \cos(p\theta) \tag{6.1}$$

A complex Fourier expansion for the displacement components in the circumferential direction can be employed whereas the mode shapes in the axial direction are the same as presented in Liu and Uras (1989a):

$$\bar{U}_n(\theta) = \bar{V}_n(\theta) = \bar{W}_n(\theta) = \exp(-jn\theta) \qquad \text{for } \delta u \tag{6.2}$$

and

$$\bar{U}_m(\theta) = \bar{V}_m(\theta) = \bar{W}_m(\theta) = \exp(jm\theta) \qquad \text{for } u \tag{6.3}$$

where $j = \sqrt{-1}$.

The analysis regarding the zeroth-order geometrical stiffness term, Eqn. (5.5) is already been presented in depth by Liu and Uras (1989a). Hence, the emphasis will be devoted to the additional first-order terms due to the existence of imperfection.

Since only the horizontal excitation is considered, the initial stresses are expected to be functions of sinθ or cosθ. The overall response of the structure is expected to be altered due to the imperfection, however, this effect is neglected in this study. Thus, the stresses of the zeroth-order response are left unchanged. Moreover, the coupling introduced by the second order terms is higher order, i.e.

hardly encountered in the experiments of Chiba et al. (1986), and is neglected. From Table 5.1, through the use of Eqn. (6.1), it can be shown that

$$B^{0}_{n\theta} \sim \exp(\pm jn\theta)$$

$$B^{1}_{n\theta} \sim \exp(\pm jn\theta)\sin(p\theta) \text{ and/or } \exp(\pm jn\theta)\cos(p\theta)$$

$$S_0 \sim \cos\theta \text{ and/or } \sin\theta$$

$$S_1 \sim \cos\theta\cos(p\theta) \text{ and/or } \sin\theta\cos(p\theta)$$

where a tilde identifies the terms associated with the circumferential direction. The resulting integrals can be summarized as:

$$I = \int_0^{2\pi} \exp(-jn\theta) \begin{Bmatrix}\cos\theta \\ \sin\theta\end{Bmatrix} \exp(jm\theta) \begin{Bmatrix}\cos(p\theta) \\ \sin(p\theta)\end{Bmatrix} d\theta \qquad (6.4)$$

The orthogonality of the sinuzoidal functions yields the following coupling among the circumferential modes

(i) n and n+p+1

(ii) n and n+p-1

(iii) n and n-p+1

(iv) n and n-p-1

The form of imperfection, characterized by p, gives rise to additional coupling regions in the buckling analysis. Hence, a qualitative study on the choice of p reveals the following conclusion:

The case, where p=0, yields no significant information, since it represents the case in which the radius differs from the original one by a constant amount.
For p=1 case, the additional modal couplings are identified as (n,n) and (n,n+2). The appearance of the uncoupled mode case, i.e. (n,n), is a curious outcome, since these regions are expected to arise only if there is vertical ground motion. An inspection of the spectra from the experiments by Chiba et al. (1986) shows that (n,n) type of modes have been encountered. A possible explanation is that, although small in amplitude, an imperfection can introduce additional instability regions.
The cases where p>1 different coupling combinations are identified, however, the experimental spectrum hardly shows any effects of these.

For failure conditions in which the buckling modes are not exactly known from the shaking table experiments, the significant bifurcation solutions can be identified from the analysis presented by Liu and Uras (1989a). The present study extends the applicability of the above-mentioned analysis to liquid-filled shells with geometrical imperfections.

Acknowledgement

The support of National Science Foundation Grant No. CES-8614957 is gratefully acknowledged.

References

Chiba, M., Tani, J., Hashimoto H. and Sudo S., "Dynamic Stability of liquid-filled cylindrical shells under horizontal excitation, Part I: Experiment," Journal of Sound and Vibration 104, 301-319 (1986).

Koiter, W. T., "On the nonlinear theory of thin elastic shells," Proceedings of the Royal Netherlands Academy of Sciences, Series B, 69, 1-54 (1966).

Liu, W. K. and Uras, R. A., "Transient failure analysis of liquid-filled shells. Part I : Theory," accepted for publication in Nuclear Engineering and Design (1989a).

Liu, W. K. and Uras, R. A., "Transient failure analysis of liquid-filled shells. Part II : Applications," accepted for publication in Nuclear Engineering and Design (1989b).

Sanders, J. L., "Nonlinear theories for thin shells," Quarterly Applied Mathematics 21, 21-36 (1963).

Uras, R. A. and Liu W. K., "Dynamic buckling of liquid-filled shells under horizontal excitation," accepted for publication in Journal of Sound and Vibration (1990).

$B_{n\theta} =$

$$\begin{bmatrix} \overline{U}_n & 0 & 0 & \overline{U}_n\Gamma^1_{11} & \overline{V}_n\Gamma^1_{21} & -\overline{W}_n b^1_1 \\ 0 & \overline{V}_n & 0 & \overline{U}_n\Gamma^2_{11} & \overline{V}_n\Gamma^2_{21} & -\overline{W}_n b^2_1 \\ 0 & 0 & \overline{W}_n & \overline{U}_n b_{11} & \overline{V}_n b_{21} & 0 \\ 0 & 0 & 0 & \overline{U}_{n,\theta}+\overline{U}_n\Gamma^1_{12} & \overline{V}_n\Gamma^1_{22} & -\overline{W}_n b^1_2 \\ 0 & 0 & 0 & \overline{U}_n\Gamma^2_{12} & \overline{V}_{n,\theta}+\overline{V}_n\Gamma^2_{22} & -\overline{W}_n b^2_2 \\ 0 & 0 & 0 & \overline{U}_n b_{12} & \overline{V}_n b_{22} & \overline{W}_{n,\theta} \end{bmatrix}$$

$$B_{zi} = \begin{bmatrix} U_{i,z} & 0 & 0 \\ 0 & V_{i,z} & 0 \\ 0 & 0 & W_{i,z} \\ U_i & 0 & 0 \\ 0 & V_i & 0 \\ 0 & 0 & W_i \end{bmatrix}$$

$$S = \begin{bmatrix} S^{11}G & S^{12}G \\ S^{21}G & S^{22}G \end{bmatrix}$$

$$G = \begin{bmatrix} g_{11} & g_{12} & 0 \\ g_{21} & g_{22} & 0 \\ 0 & 0 & 1 \end{bmatrix}$$

Table 3.1. The explicit forms of the matrices in the geometrical stiffness matrix

	Frequency axial mode		Parameters governing the instability regions $(\varpi, \varepsilon_{cr})$; $\sigma=3.6\cdot10^{-6}$ $(\omega_{in}^2+\omega_{j,n+1}^2)$ $\zeta_{min}= 0.0001$; $\omega_{min}= 27.76$ Hz. *** represents $\varepsilon_{cr} > 0.4$			
	i=1	i=2	a	b	c	d
n	ω_{1n}	ω_{2n}	(n,n+1),(1,i) $(\varpi, \varepsilon_{cr})$	(n,n+1),(1,2) $(\varpi, \varepsilon_{cr})$	(n,n+1),(2,1) $(\varpi, \varepsilon_{cr})$	(n,n+1),(2,2) $(\varpi, \varepsilon_{cr})$
1	***115.40***	256.96	(182.90,0.31)	(328.59,***)	(324.46,***)	(470.14,***)
2	67.50	213.19	(***110.43***,0.05)	(228.45,***)	(256.12,0.19)	(374.14,0.22)
3	42.94	160.96	(74.13,0.01)	(167.25,0.08)	(192.15,0.04)	(285.27,0.10)
4	31.20	124.31	(58.96,0.00)	(131.67,0.02)	(152.08,0.02)	(224.79,0.05)
5	27.76	100.48	(58.41,0.00)	(***114.44***,0.01)	(131.12,0.02)	(187.15,0.02)
6	30.65	86.67	(67.54,0.00)	(***112.10***,0.01)	(***123.57***,0.02)	(168.13,0.01)
7	36.89	81.46	(81.37,0.01)	(***120.01***,0.02)	(125.93,0.81)	(164.58,0.01)
8	44.47	83.12	(97.45,0.01)	(132.42,0.06)	(136.10,0.07)	(171.07,0.01)
9	52.98	87.95	(***116.01***,0.01)	(147.49,0.18)	(150.99,0.10)	(182.47,0.01)
10	63.04	94.52	(138.01,0.01)	(166.40,0.17)	(169.49,1.09)	(197.88,0.01)

Table 4.1a Frequency spectrum and buckling frequencies for a 75% full tall shell

n	n+1	experimental frequencies (Hz.)	theoretical frequencies (Hz.)	% difference
5	6	58	58	0
6	7	66	67	1.51
7	8	80	81	1.25
8	9	96	97	1.04
9	10	114	116	1.75
10	11	136	138	1.47

Table 4.1b. Comparison of experimental and theoretical buckling frequencies due to (n)th and (n+1)th circumferential coupling for a 75% full tall shell

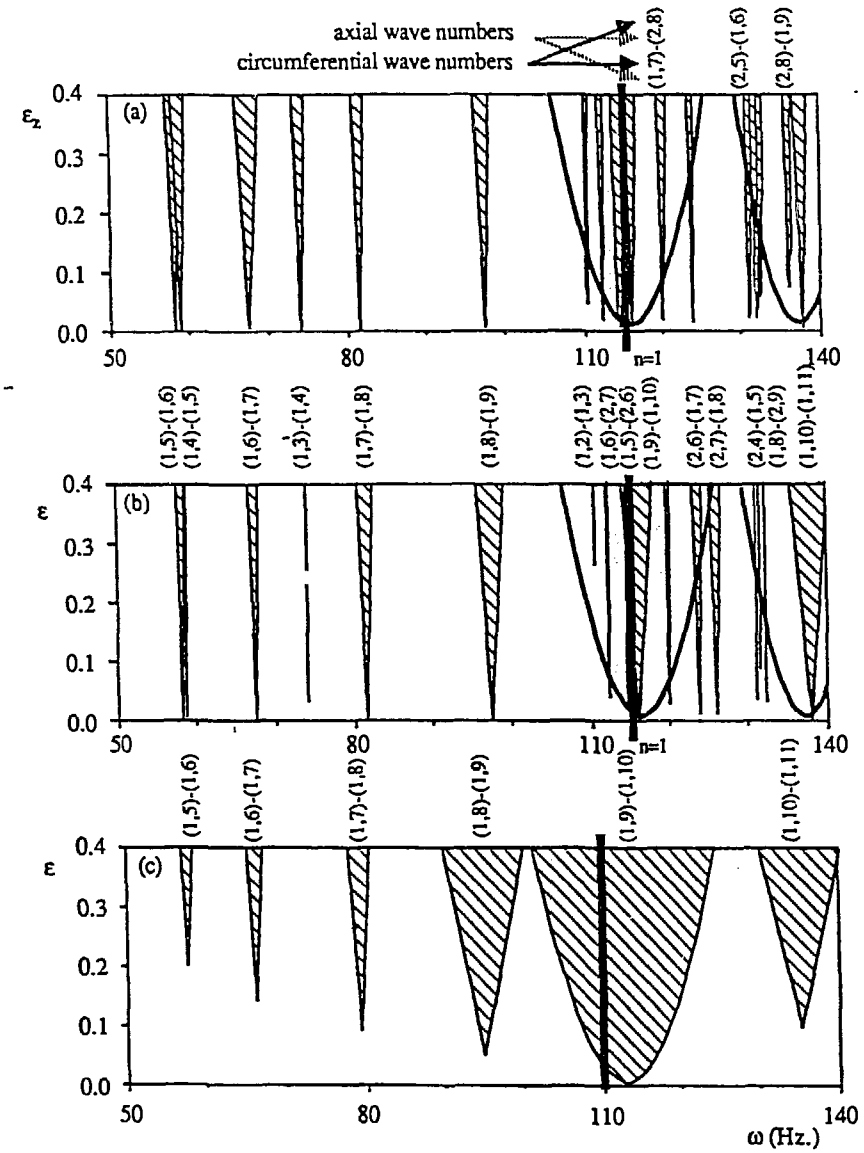

Figure 4.1. Stability charts for 75% full tall shell using: (a) the analysis by Liu and Uras (1989b); (b) the analysis Uras and Liu (1990); and (c) the experiments by Chiba et al. (1986)

Center across both columns on page 1: Title, Authors, Affiliations

Start page 1, beginning with abstract

$$
B^{0}_{n\theta} = \begin{bmatrix}
\bar U_n & 0 & 0 & 0 & 0 & 0 \\
0 & \bar V_n & 0 & 0 & 0 & 0 \\
0 & 0 & \bar W_n & 0 & 0 & 0 \\
0 & 0 & 0 & \bar U_{n,\theta} & 0 & 0 \\
0 & 0 & 0 & 0 & \bar V_{n,\theta} & -\bar W_n/\bar R \\
0 & 0 & 0 & 0 & \bar V_n \bar R & \bar W_{n,\theta}
\end{bmatrix}
$$

$$
B^{1}_{n\theta} = \begin{bmatrix}
0 & 0 & 0 & 0 & 0 & 0 \\
0 & 0 & 0 & 0 & 0 & 0 \\
0 & 0 & 0 & 0 & 0 & 0 \\
0 & 0 & 0 & 0 & 0 & 0 \\
0 & 0 & 0 & 0 & \bar V_n A_1 & -\bar W_n A_3 \\
0 & 0 & 0 & 0 & \bar V_n A_2 & 0
\end{bmatrix}
$$

$A_1 = f_{,\theta}$

$A_2 = \bar R\,(f - f_{,\theta\theta})$

$A_3 = -(f + f_{,\theta\theta})/\bar R$

$$
B^{2}_{n\theta} = \begin{bmatrix}
0 & 0 & 0 & 0 & 0 & 0 \\
0 & 0 & 0 & 0 & 0 & 0 \\
0 & 0 & 0 & 0 & 0 & 0 \\
0 & 0 & 0 & 0 & 0 & 0 \\
0 & 0 & 0 & 0 & \bar V_n A_1 & -\bar W_n A_3 \\
0 & 0 & 0 & 0 & \bar V_n A_2 & 0
\end{bmatrix}
$$

$A_1 = f_{,\theta}\,(f_{,\theta\theta} - f)$

$A_2 = \bar R\,(-f^2 + \frac{5}{2} f_{,\theta}^2)$

$A_3 = (-f^2 + 4 f f_{,\theta\theta} + \frac{1}{2} f_{,\theta}^2)/\bar R$

$$
S_0 = \begin{bmatrix} S_0^{11}\bar G_0 & S_0^{12}\bar G_0 \\ S_0^{21}\bar G_0 & S_0^{22}\bar G_0 \end{bmatrix}
$$

$$
S_1 = \begin{bmatrix} S_1^{11}\bar G_0 & S_1^{12}\bar G_0 \\ S_1^{21}\bar G_0 & S_1^{22}\bar G_0 \end{bmatrix} + \begin{bmatrix} S_0^{11}\bar G_1 & S_0^{12}\bar G_1 \\ S_0^{21}\bar G_1 & S_0^{22}\bar G_1 \end{bmatrix}
$$

$$
S_2 = \begin{bmatrix} S_2^{11}\bar G_0 & S_2^{12}\bar G_0 \\ S_2^{21}\bar G_0 & S_2^{22}\bar G_0 \end{bmatrix} + \begin{bmatrix} S_1^{11}\bar G_1 & S_1^{12}\bar G_1 \\ S_1^{21}\bar G_1 & S_1^{22}\bar G_1 \end{bmatrix} + \begin{bmatrix} S_0^{11}\bar G_2 & S_0^{12}\bar G_2 \\ S_0^{21}\bar G_2 & S_0^{22}\bar G_2 \end{bmatrix}
$$

$$
\bar G_0 = \bar R \begin{bmatrix} 1 & 0 & 0 \\ 0 & \bar R^2 & 0 \\ 0 & 0 & 1 \end{bmatrix} \qquad \bar G_1 = f\,\bar G_0 \qquad \bar G_2 = \frac{1}{2} f_{,\theta}^2\,\bar R \begin{bmatrix} 1 & 0 & 0 \\ 0 & 3\bar R^2 & 0 \\ 0 & 0 & 1 \end{bmatrix}
$$

Table 5.1. Explicit forms of the matrices up to the second-order